Optimizing Association of Heteronuclear Feshbach Molecules in Microgravity with a Magnetic Field Quench

by

Kirk S. Waiblinger

B.A., Physics, University of Colorado Boulder

Defense Date: April 3rd, 2019

Research Advisor: Dr. Jose P. D'Incao (Physics)

Honors Council Representative: Dr. John P. Cumalat (Physics)

Extradepartmental Reader: Dr. Markus J. Pflaum (Mathematics)

Committee Member: Dr. Andreas Becker (Physics)

A thesis submitted to the faculty of the
University of Colorado in partial fulfillment
of the requirements for the designation of
Latin Honors in the Department of Physics
2019

This thesis entitled:
Optimizing Association of Heteronuclear Feshbach Molecules in Microgravity with a Magnetic Field Quench
written by Kirk S. Waiblinger
has been approved for the Department of Physics

Prof. Jose P. D'Incao

Prof. John P. Cumalat

Prof. Markus J. Pflaum

Prof. Andreas Becker

Date _____

The final copy of this thesis has been examined by the signatories, and we find that both the content and the form meet acceptable presentation standards of scholarly work in the above mentioned discipline.

Waiblinger, Kirk S. (B.A., Physics)

Optimizing Association of Heteronuclear Feshbach Molecules in Microgravity with a Magnetic Field Quench

Thesis directed by Prof. Jose P. D'Incao

This work presents a computational comparison of two magnetic field manipulation schemes for creating heteronuclear ^{87}Rb^{41}K Feshbach molecules. We focus on analysis of the parameters relevant to the NASA Cold Atom Laboratory experiments performing atom interferometry, which will require maximizing production of molecules at low densities, and extremely low temperatures (< 1 nK). It is found that a scheme involving a magnetic field quench potentially offers substantial benefits over a direct linear magnetic field sweep across a Feshbach resonance.

Acknowledgements

Thank you to all the people that I have to thank for encouraging me to excel and keeping me afloat throughout my time at CU. To my family for their constant support. To my close friends for making every lecture in physics and every homework session a pleasure. To my many outstanding professors for teaching me more than I ever knew there was to learn. And to my mentor Jose, for having expertly mentored me from before I had taken a day's worth of quantum mechanics or numerical analysis all the way through the complexity of the topics in this thesis.

Contents

Chapter

Chapter 1

Introduction

Currently aboard the International Space Station is a multi-user facility known as the Cold Atom Laboratory (CAL), whose purpose is to study ultracold atoms in microgravity, and the applications that they have for fundamental sciences and precision measurement. Due to the microgravity environment, lifetimes of ultracold gases of 10 seconds or more, and temperatures below 100 pK are achievable, significantly improving on Earth-bound experiments [1]. The experiment which we will analyze is a proposal to perform atom interferometry using two species of ultracold atoms, which would enable tests of the Weak Equivalence Principle (WEP), the principle from classical gravity and general relativity that inertial mass, i.e. the mass appearing in $\sum \mathbf{F} = m\mathbf{a}$, is the same as gravitational mass, i.e. the mass appearing in $\mathbf{F} = m\mathbf{g}$, with $\mathbf{g}$ representing a gravitational field. It may be seen that the Universality of Free Fall (UFF), the well-known principle that any two bodies have the same acceleration in a gravitational field, is equivalent to the WEP.

No violation of the WEP has been observed to date, however, several proposed quantum gravity theories predict small violations of the WEP [2, 3]. The NASA CAL facility will attempt to verify the WEP at these levels, through dual-species atom interferometry techniques (see Fig. 1.1). Testing the WEP at the precision it is predicted to be violated requires production of clouds of two species of atoms (^{87}Rb and ^{41}K will be used) with common centers of mass, to within nm-accuracy [4].

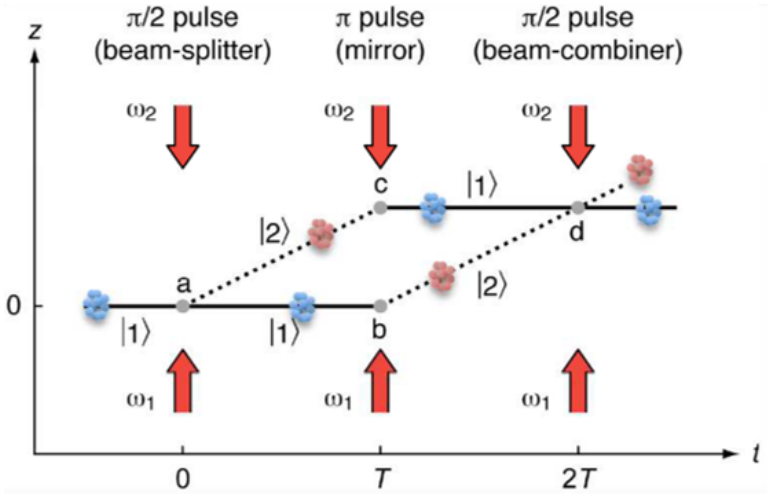

Figure 1.1: A schematic of atom interferometry, used with permission from [5]. An initial cloud of ultracold atoms is spatially separated into a coherent superposition of spatially distinct components at point a. During the free evolution of the components, between $t = 0$ and $t = T$ and between $t = T$ and $t = 2T$, the spatially separated components acquire a phase determined by the forces acting on them. At point d, the components of the system are recombined, exhibiting an interference pattern that can be measured. In the NASA CAL experiment the initial cloud will be composed of two species of atoms, ^{87}Rb and ^{41}K.

The following scheme has been proposed for creating such clouds with high-accuracy common centers of mass [4]. One begins with the system in a state consisting purely of free atoms. Then, bonding exclusively between pairs of Rb and K atoms is induced. When all remaining free atoms have been expelled, one breaks all bonds between Rb-K pairs, leaving the desired overlapping Rb and K clouds, illustrated in Fig. 1.2.

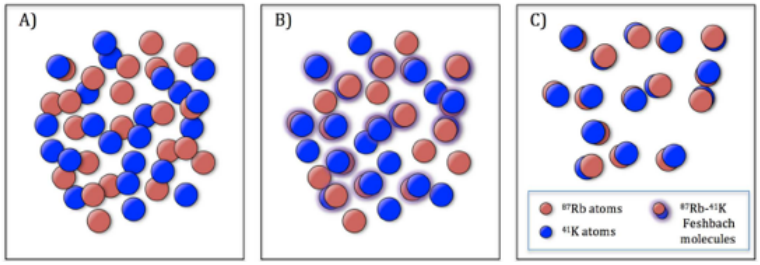

Figure 1.2: A schematic for creation of common-cm clouds of ^{87}Rb and ^{4}1K atoms, used with permission from [5]. In A), an initial cloud of free Rb and K atoms is created. Then, bonding between Rb-K pairs is induced in B), creating molecules. After expelling free atoms, and breaking molecular bonds between Rb-K pairs, the resulting system in C) is composed of free Rb and K atoms with highly correlated center of mass.

We are concerned exclusively with the first part of this process; the goal of this thesis is to analyze schemes to maximize the number of Rb-K pairs produced from an ultracold gas consisting of free Rb and K atoms. To this end, we provide a computational comparison of two feasible schemes to produce RbK molecules via magnetically tunable interactions between atoms that occur as a result of Feshbach resonances. Our analysis allows us to determine the most efficient scheme to produce such molecules in the unique experimental conditions provided by the CAL's microgravity environment.

Chapter 2

Theoretical Background

In this chapter, we give an overview of some of the theoretical principles underlying this work. In order to study formation of molecules at zero temperature, the major theoretical subjects involved will be Bose-Einstein condensation, low-energy scattering processes, and atomic interactions via Feshbach resonance. Since each of these topics is extremely vast, we confine the discussion for the most part to the aspects most relevant to our study.

2.1 Bose-Einstein Condensation

At extremely low temperatures, atoms behave in novel ways that allow experimenters to fully control the fundamental interatomic interactions and make extraordinarily precise measurements. This is due to sudden phase transitions from ordinary thermal gases of particles to regimes in which macroscopic quantum effects define the collective behavior of particles. In the case of ^{87}Rb and ^{41}K, both are bosonic particles (particles having integer spin), whose quantum regimes exhibit the phenomenon of Bose-Einstein condensation.

2.1.1 Bose-Einstein Distribution

We begin by introducing the theory of Bose-Einstein condensation, largely following the derivations in references [6, 7]. We shall first derive the Bose-Einstein distribution, then discuss how this leads to condensation.

Recall from statistical mechanics the grand partition function for a system consisting of a single species of particles,

$$\mathcal{Z} = \sum_s \exp\left[\frac{-(E(s) - \mu N(s))}{k_B T}\right], \tag{2.1}$$

where the summation is taken over all available states s of a system, $E(s)$ is the energy of each state, μ the chemical potential, $N(s)$ is the number of particles in the state, k_B the Boltzmann constant, and T the temperature. Each term in the summation is known as the Gibbs factor for the state, which has the property that the probability of the state being occupied is simply the ratio of its Gibbs factor to the partition function. When considering a single-particle state with energy ϵ that may be occupied by an arbitrary number n of indistinguishable, noninteracting bosons (note the absence of any combinatorial terms), the partition function becomes

$$\begin{aligned}
\mathcal{Z} &= \sum_{n\in\mathbb{N}} \exp\left[\frac{-(n\epsilon - \mu n)}{k_B T}\right] \\
\mathcal{Z} &= \sum_{n\in\mathbb{N}} \left(\exp\left[\frac{-(\epsilon - \mu)}{k_B T}\right]\right)^n \\
\mathcal{Z} &= \frac{1}{1 - \exp\left[\frac{-(\epsilon-\mu)}{k_B T}\right]},
\end{aligned}$$

where, in the last line, we have resolved the summation by identifying the Taylor expansion $\frac{1}{1-x} = \sum_{n\in\mathbb{N}} x^n$, noting that we have $\epsilon > \mu$, so the summation is convergent. We can use this to evaluate the probability of a given number of particles occupying a state, using the fact that the probability of a given state being occupied is simply the ratio of its Gibbs factor to the partition function,

$$P(n) = \frac{\exp\left[\frac{-n(\epsilon-\mu)}{k_B T}\right]}{1 - \exp\left[\frac{-(\epsilon-\mu)}{k_B T}\right]}. \tag{2.2}$$

Now, in order to find the mean occupation number of the state, $\overline{n}$, we shall evaluate

$$\begin{aligned}
\overline{n} &= \sum_{n\in\mathbb{N}} nP(n) \\
\overline{n} &= \sum_{n\in\mathbb{N}} \frac{n \exp\left[\frac{-n(\epsilon-\mu)}{k_B T}\right]}{1-\exp\left[\frac{-(\epsilon-\mu)}{k_B T}\right]} \\
\overline{n} &= \frac{1}{\exp\left[\frac{\epsilon-\mu}{k_B T}\right]-1},
\end{aligned}$$

which is the well-known Bose-Einstein distribution[1] :

$$\overline{n}_{BE}(\epsilon; T, \mu) = \frac{1}{\exp\left[\frac{\epsilon-\mu}{k_B T}\right]-1}. \tag{2.3}$$

In Fig. 2.1, one can see that the mean number of particles in a particular state increases as μ approaches ϵ, and as $T \to 0$.

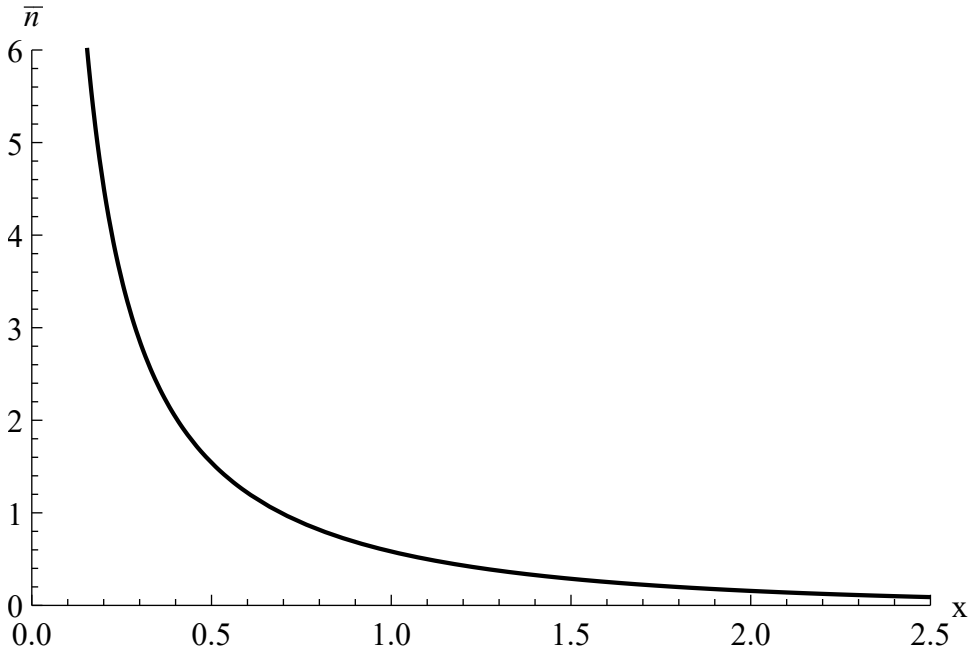

Figure 2.1: The Bose-Einstein distribution, with $x = \frac{\epsilon-\mu}{k_B T}$. Note that $x < 0$ would correspond to $\mu > \epsilon$, which is unphysical.

[1] To resolve the final summation, an easy method is to set $x = (\epsilon - \mu)/k_B T$, and note that $\overline{n} = \sum n \frac{\exp(-nx)}{\mathcal{Z}} = -\frac{1}{\mathcal{Z}} \sum \frac{\partial}{\partial x} \exp(-nx) = -\frac{1}{\mathcal{Z}} \frac{\partial}{\partial x} \sum \exp(-nx) = -\frac{1}{\mathcal{Z}} \frac{\partial \mathcal{Z}}{\partial x}$

2.1.2 Transition Temperature

In principle, if the temperature and chemical potential of a system are given, Eq. (2.3) allows us to calculate the occupation number of a given state. Unfortunately, however, the temperature and chemical potential are not independent and generally only the temperature is known. So, we shall take as given the temperature, and calculate the chemical potential, which depends nontrivially on temperature, particle number, and confining potential of a system. In particular, the chemical potential is determined by the constraint that the mean occupation numbers of all single-particle states sum to the fixed, total number of particles in the system, in other words,

$$\begin{aligned} N &= \sum_s \overline{n}_{BE}(\epsilon(s); T, \mu) \\ &= \sum_s \frac{1}{\exp\left[\frac{\epsilon(s)-\mu}{k_B T}\right] - 1}. \end{aligned}$$

This sum is not generally tractable, but it may be simplified by introducing a continuous density of states $g(\epsilon)$, determined by the particular confining potential, and reformulating the summation as an integral, yielding

$$N = N_0 + \int_{0^+}^{\infty} d\epsilon \left(g(\epsilon) \frac{1}{\exp\left[\frac{\epsilon-\mu}{k_B T}\right] - 1} \right), \tag{2.4}$$

in which the ground state energy has been chosen to be 0 (or, more precisely, a small positive quantity such that $\epsilon_{min} \ll k_B T$. We have separated the ground-state occupancy $N_0 \approx \frac{1}{\exp\left[-\frac{\mu}{k_B T}\right]-1}$ from the integral because continuous densities of states fail to accurately represent discrete spectra at $\epsilon = 0$, where physical spectra are sparse. In particular, densities of states generally go to 0 as $\epsilon \to 0$, neglecting any contribution due to the ground state with $\epsilon \approx 0$ [6, 7]. For a given confining potential, Eq. (2.4) could be solved numerically to find μ.

Ultimately, however, we are more interested in N_0 than in μ for the purposes of Bose-Einstein condensation. In order to estimate the transition temperature T_C below which the

number of condensed atoms N_0 becomes non-negligible, we suppose $N_0 = 0$, then determine the minimal temperature at which there exists a value of the chemical potential such that the integral for the number of particles in excited states equals the total number of particles. In other words, we will find the minimal T such that

$$N = N_{exc}(T, \mu) = \int_{0^+}^{\infty} d\epsilon \left(g(\epsilon) \frac{1}{\exp\left[\frac{\epsilon - \mu}{k_B T}\right] - 1} \right).$$

for some value of μ. It is straightforward to observe that $N_{exc}(T, \mu)$ increases with μ. Since $\mu \leq \epsilon$ for all ϵ, and $\epsilon_{min} \approx 0$, we find that the minimum temperature at which N_0 is negligible occurs when $\mu = 0$, implying the condition

$$N = N_{exc}(T_C, \mu = 0). \tag{2.5}$$

To demonstrate a model computation of T_C, we shall use a 3D square well potential, with density of states given by[2] $g(\epsilon) = \left(\frac{m^{3/2}}{\pi^2 \sqrt{2} \hbar^2}\right) V \sqrt{\epsilon}$, in which V is the confining volume, m the mass of a single particle, and $\hbar$ the reduced Planck constant, or simply $g(\epsilon) = C\sqrt{\epsilon}$, with C representing the appropriate constants [6]. We have

$$\begin{aligned} N_{exc}(T, \mu = 0) &= \int_{0^+}^{\infty} d\epsilon \frac{C\sqrt{\epsilon}}{\exp\left[\epsilon / k_B T\right] - 1} \\ &= C(k_B T)^{3/2} \int_{0^+}^{\infty} dx \frac{\sqrt{x}}{\exp x - 1} \\ &= C\left(k_B T\right)^{3/2} \Gamma(3/2)\zeta(3/2) \\ &\approx 2.315 C(k_B T)^{3/2} \end{aligned} \tag{2.6}$$

after evaluating the integral numerically[3] . Setting $N = N_{exc}$ at T_C, evaluating pure numerical factors and introducing the number density $n = N/V$, we find

$$k_B T_C \approx 3.31 \frac{\hbar^2 n^{2/3}}{m}. \tag{2.7}$$

[2] Note that at $\epsilon = 0$ this gives a density of states of 0, effectively ignoring the ground state as previously claimed, hence the importance of counting the ground state separately.

[3] In general, one has $\int_0^\infty \frac{t^{\alpha-1}}{\exp x - 1} = \Gamma(\alpha)\zeta(\alpha)$ for $\operatorname{Re}\alpha > 1$, with Γ the gamma function and ζ the Riemann zeta function [7].

Additionally, the result that $N_{exc}(T, \mu = 0) \propto T^{3/2}$ in Eq. (2.6), combined with the constraint that $N = N_0 + N_{exc}$ immediately yields the convenient relations

$$N_{exc} \approx \left(\frac{T}{T_C}\right)^{3/2} N \tag{2.8}$$

$$N_0 \approx \left[1 - \left(\frac{T}{T_C}\right)^{3/2}\right] N \tag{2.9}$$

when $T < T_C$ (since then $\mu = 0$). This striking behavior, that below a certain temperature T_C the many-particle system quickly collapses into a collection of particles mostly inhabiting the same state, is the defining feature of Bose-Einstein condensation.

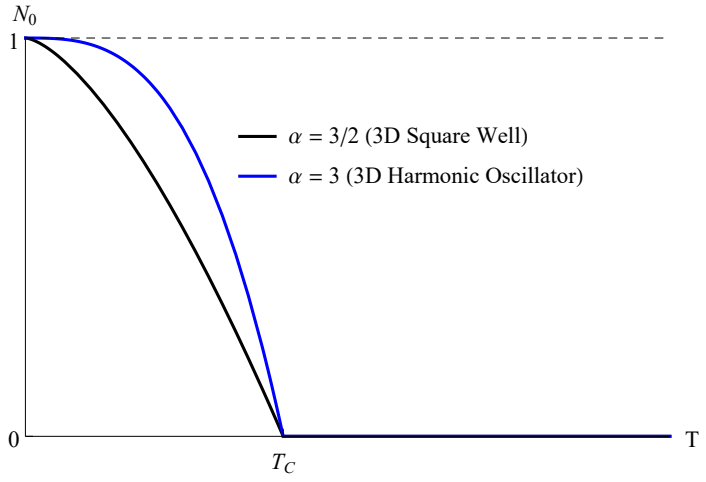

Figure 2.2: Condensate fraction as a function of temperature relative to T_C

Although these results were derived with a 3D square well potential, we mention for completeness that any confining potential with $g(\epsilon) \propto \epsilon^{\alpha-1}$, $\alpha > 1$, will have $N_{exc}(T, \mu = 0) \propto T^{\alpha}$, and therefore exhibit the same condensation phenomenon [7], only with a different exponent, namely

$$N_0 \approx \left[1 - \left(\frac{T}{T_C}\right)^{\alpha}\right] N. \tag{2.10}$$

For instance, the other ubiquitous potential, the 3D harmonic oscillator, has $\alpha = 3$. Fig. 2.2 shows the relationship between N_0 and T for both of those potentials. One can see quite clearly that one has $N_0 \to 1$ as $T \to 0$, in each case, which is also true for any $\alpha > 1$ [7].

Therefore, when we model Bose-Einstein condensates (BECs) at zero temperature, we will assume an initial state with 100% of atoms populating the ground state. Lastly, we mention that there are physical potentials resulting in densities of states with $\alpha \leq 1$, such as the 2D harmonic oscillator, but these are not capable of exhibiting condensation [7].

2.2 Low-Energy Scattering

Throughout Sec. 2.1, we assumed that all atoms in a BEC were noninteracting and independent. However, real atoms do interact, of course, and in this study we are quite interested in the interactions, since they are responsible for forming molecules. Therefore, in this section, we establish some of the simplifying assumptions used to model the low-energy scattering processes in a BEC. Because the particles within a BEC are each assumed to be in their ground state, we are interested in understanding their interactions in the zero-energy limit, $E = \frac{\hbar^2 k^2}{2\mu} \to 0$, or, equivalently, when the relative momentum between particles tends to 0, $k \to 0$. In the following discussion, we appeal to an intuitive physical argument, although we note that far more comprehensive and rigorous asymptotic analyses can be and have been done (see e.g. Refs. [7, 8]).

2.2.1 Central Potential

Consider two distinguishable particles in free space interacting through a potential V, which depends only on the distance between them (known as a "central potential"). Then, the time-independent Schrödinger equation, $\hat{H}\,|\psi\rangle = E\,|\psi\rangle$ may be written [9] as

$$\left[\frac{\hat{\mathbf{p}}_1^2}{2m_1} + \frac{\hat{\mathbf{p}}_2^2}{2m_2} + \hat{V}(|\mathbf{r}_2 - \mathbf{r}_1|)\right]\psi(\mathbf{r}_1, \mathbf{r}_2) = E\psi(\mathbf{r}_1, \mathbf{r}_2). \tag{2.11}$$

We suppose $\psi(\mathbf{r}_1, \mathbf{r}_2) = \psi_{CM}(\mathbf{R})\psi_{rel}(\mathbf{r})$, where we have defined center of mass and relative coordinates, namely $\mathbf{r} = \mathbf{r}_2 - \mathbf{r}_1$ and $\mathbf{R} = \frac{m_1\mathbf{r}_1 + m_2\mathbf{r}_2}{m_1+m_2}$. We also define total mass $M = m_1 + m_2$ and reduced mass $\mu = \frac{m_1 m_2}{m_1+m_2}$. By applying the canonical substitution $\hat{\mathbf{p}} \to i\hbar\nabla$, it may be

proven that the system Hamiltonian may be rewritten in fully separable form as

$$\hat{H} = \left(\frac{\hat{\mathbf{P}}^2}{2M}\right) + \left(\frac{\hat{\mathbf{p}}^2}{2\mu} + \hat{V}(r)\right) \tag{2.12}$$

$$= \hat{H}_{CM} + \hat{H}_{rel} \tag{2.13}$$

in which the momentum operators represent derivatives with respect to the corresponding transformed coordinates. Treating the center of mass motion first, we solve the corresponding Schrödinger equation:

$$\frac{\hat{\mathbf{P}}^2}{2M}\psi_{CM}(\mathbf{R}) = E_{CM}\psi_{CM}(\mathbf{R}) \tag{2.14}$$

$$\implies -\frac{\hbar^2\nabla_R^2}{2M}\psi_{CM}(\mathbf{R}) = E_{CM}\psi_{CM}(\mathbf{R}) \tag{2.15}$$

$$\implies \psi_{CM}(\mathbf{R}) = \exp(i\mathbf{K}\cdot\mathbf{R}), \tag{2.16}$$

satisfying $E_{CM} = \frac{\hbar^2 K^2}{2M}$, and where we will not be particular about normalization of continuum states. This is a plane wave state that is independent of the scattering potential, and therefore unimportant to all following discussion.

We turn now to the relative motion, with Hamiltonian

$$\hat{H} = \frac{\hat{\mathbf{p}}^2}{2\mu} + \hat{V}(r). \tag{2.17}$$

Note that we drop the subscripts for relative motion, since this is the only part of the wavefunction that will concern us from now on. After substituting the Laplacian in spherical coordinates, one finds that the Hamiltonian may be further rewritten

$$\hat{H} = -\frac{\hbar^2}{2\mu}\frac{1}{r}\frac{\partial^2}{\partial r^2}r + \frac{1}{2\mu r^2}\hat{\mathbf{L}}^2 + \hat{V}(r). \tag{2.18}$$

Observing that this equation depends on angular coordinates only through the angular momentum operator simplifies our task greatly. We write $\psi(\mathbf{r}) = f(r)Y_l^m(\theta,\phi)$, where $Y_l^m(\theta,\phi)$ are the usual spherical harmonics, and apply the Schrödinger equation again, using the

well-known eigenvalues of the spherical harmonics, $\hat{\mathbf{L}}^2 Y_l^m(\theta,\phi) = \hbar^2 l(l+1) Y_l^m(\theta,\phi)$ [9]:

$$\left[-\frac{\hbar^2}{2\mu}\frac{1}{r}\frac{\partial^2}{\partial r^2}r + \frac{1}{2\mu r^2}\hat{\mathbf{L}}^2 + V(r)\right] f(r)Y_l^m(\theta,\phi) = Ef(r)Y_l^m(\theta,\phi) \tag{2.19}$$

$$Y_l^m(\theta,\phi)\left[-\frac{\hbar^2}{2\mu}\frac{1}{r}\frac{\partial^2}{\partial r^2}r + \frac{\hbar^2}{2\mu r^2}l(l+1) + V(r)\right] f(r) \quad = Ef(r)Y_l^m(\theta,\phi) \tag{2.20}$$

$$\left[-\frac{\hbar^2}{2\mu}\frac{1}{r}\frac{\partial^2}{\partial r^2}r + \frac{\hbar^2}{2\mu r^2}l(l+1) + V(r)\right] f(r) \quad = Ef(r) \tag{2.21}$$

which is the radial Schrödinger equation. To understand low-energy scattering, it will be valuable to recast Eq. (2.21) in the form

$$\left[-\frac{\hbar^2}{2\mu}\frac{1}{r}\frac{\partial^2}{\partial r^2}r + V_{eff}^l(r)\right] f(r) = Ef(r), \tag{2.22}$$

with $V_{eff}^l(r) = \frac{\hbar^2}{2\mu r^2}l(l+1) + V(r)$. For us, Eq. (2.22) will be the fundamental equation governing time-independent scattering processes.

2.2.2 S-wave scattering

By analogy to the naming conventions for atomic orbitals, scattering processes with angular momentum quantum number $l = 0, 1, 2$, etc. are referred to as s-wave, p-wave, d-wave, etc. processes [7]. We will argue that in the limit of zero relative momentum, only s-wave processes contribute to the long-range behavior, and particularly, formation of molecules.

Generally speaking, interaction potentials $V(r)$ will take the form of a steep repulsion at short interatomic distance, followed by a potential well, which will asymptote to 0 from below [7], such as in Fig. 2.3. Note that for $l = 0$, this implies that the potential well is energetically accessible to particles even at zero energy. However, for any $l \neq 0$, the effective potential has a repulsive centrifugal barrier, which must be tunneled through in order to access the potential well, as shown in Fig. 2.4. As $k \to 0$, the corresponding tunnelling probability approaches 0 [9], meaning that the particles do not interact via non-s-wave processes.

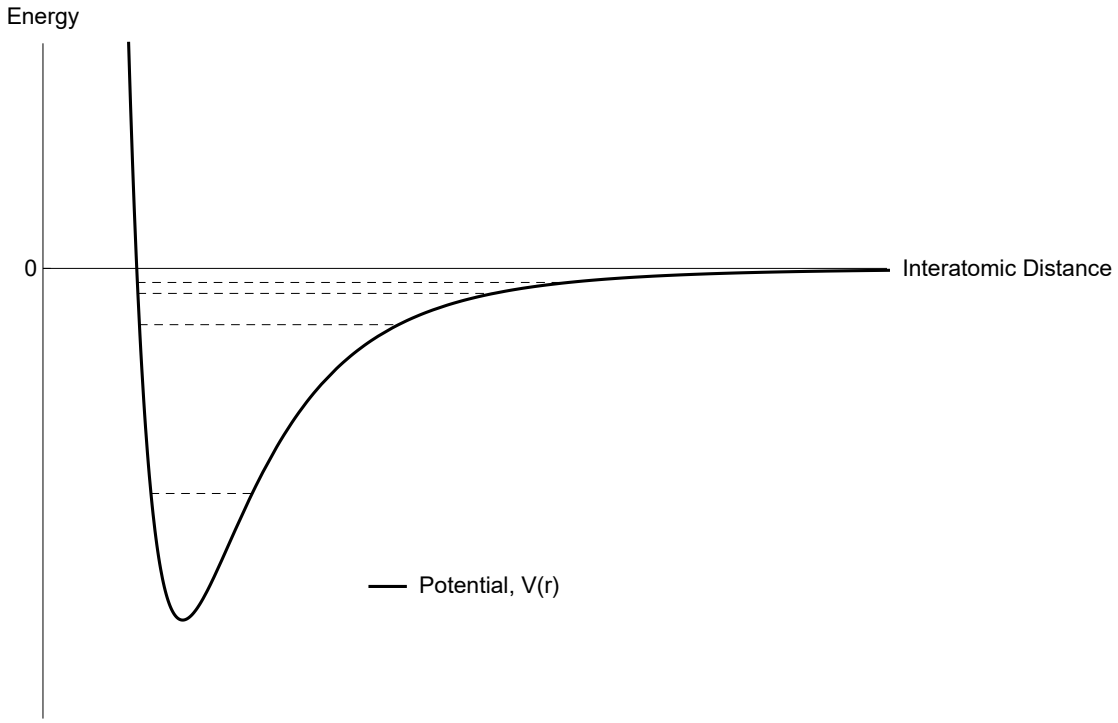

Figure 2.3: Typical shape of interaction potential between atoms, with short-range repulsion and potential well. The dashed lines represent possible bound states.

With this in mind, we make a few qualitative arguments to summarize the analysis in Ref. [7]. The relative motion in a scattering process may be described by an ansatz wavefunction of the form

$$\psi(\mathbf{r}) = \exp(ikz) + \psi_{sc}(\mathbf{r}), \tag{2.23}$$

representing the momentum plane wave of the particles' approach, taken to be in the z-direction and the wave with which they scatter off one another[4] . Spherical symmetry in the scattering potential implies azimuthal symmetry in the scattered wave, and at large r, the particles are assumed to be noninteracting for our purposes, so we can write the scattered wave as

$$\psi_{sc}(r,\theta) \sim f(\theta)\frac{\exp(ikr)}{r}, r \to \infty \tag{2.24}$$

which asymptotically solves the radial wave equation. Upon assuming pure s-wave interac-

[4] Since these are, generally, continuum states, we shall not bother with normalization

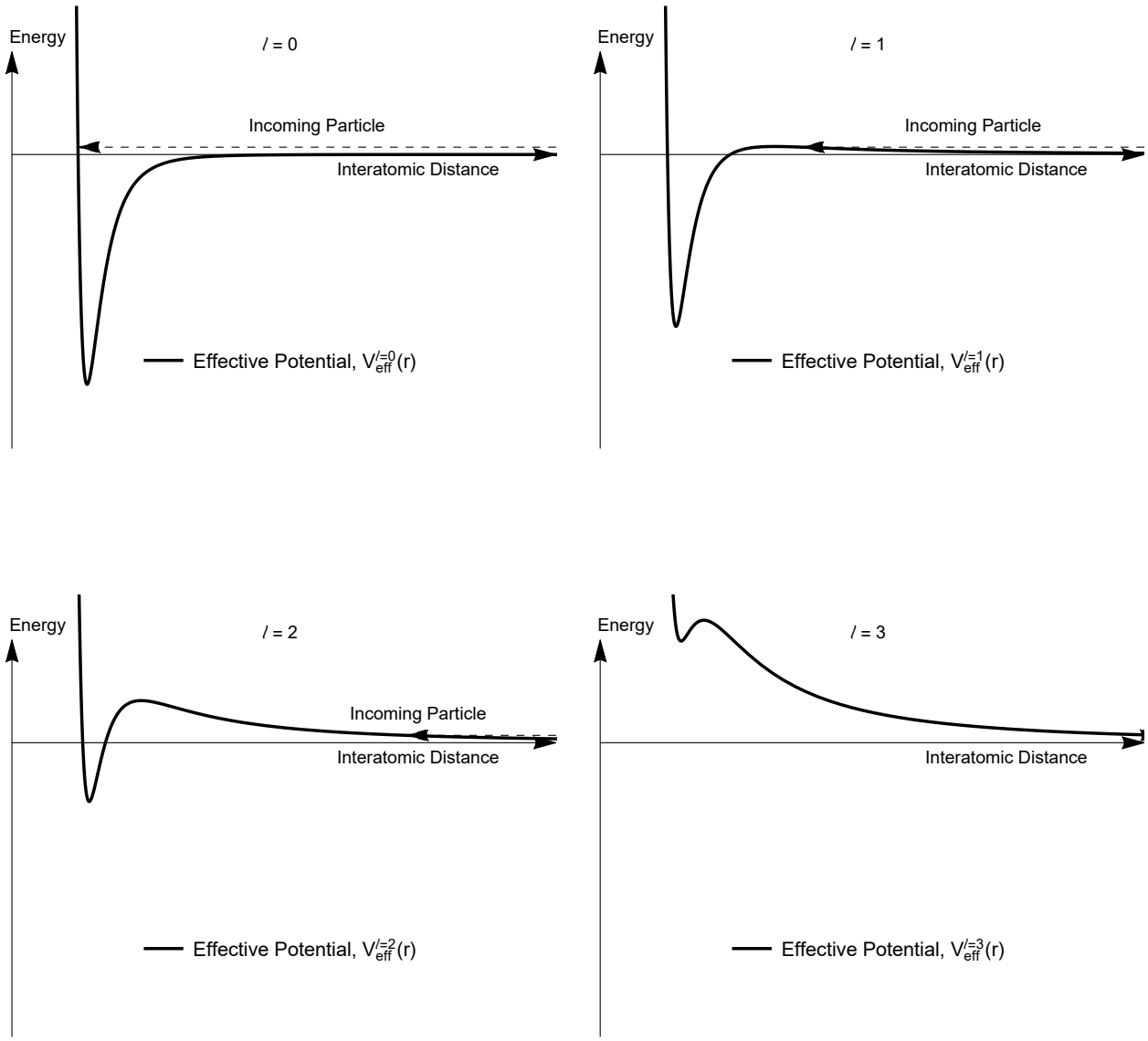

Figure 2.4: Semiclassical analogy for scattering at low energy. If one considers an incoming particle with sufficiently low energy, its classical turning points forbid it to interact with the binding potential well due to the centrifugal barrier for $l \neq 0$. Therefore we expect that the incoming plane wave has negligible projection onto the bound state. Note that for $l = 3$ the classical turning point does not even appear on the same scale.

tion, which imposes spherical symmetry on the scattered wave, and applying the low-energy

limit $kr \to 0$ the asymptotic wavefunction becomes simply

$$\psi(\mathbf{r}) = 1 - \frac{a}{r}, \tag{2.25}$$

and the scattering process is determined entirely by the real parameter a, known as the (s-wave) scattering length[5] . The scattering length is an extremely important parameter of the system; its magnitude describes the strength of interactions between atoms, among many other properties of the scattering process. For instance, one may show that the total scattering cross section is given simply by

$$\sigma = 4\pi a^2 \tag{2.26}$$

2.2.3 Universality

The most crucial result of the two previous sections is that short-range, low-energy scattering processes are, to first approximation, *entirely* determined by the scattering length. As a result, when modelling a 2-body scattering problem, different potentials give the same results, granting us significant flexibility when performing computations [7, 10]. One very general result is that for a system with $a \to +\infty$, there exists a weakly bound state with binding energy given by $E_B = \frac{\hbar^2}{2\mu a^2} + O(k^2)$ [7, 10]. This is straightforward to verify for some simple potentials, such a spherical finite square well, and, importantly for our purposes, can be shown for to be true for a scattering potential given by a van der Waals expansion [7]

$$V(r) = -\frac{C_6}{r^6} - \frac{C_8}{r^8} - \frac{C_{10}}{r^{10}} + \dots \tag{2.27}$$

Therefore, as long as we know the scattering length for a low-energy scattering process, we may substitute another, simpler potential which has the same scattering length and expect to find the same results.

[5] The scattering length is formally defined by the limit $-\frac{1}{a} = \lim_{k\to 0} k\cot(\delta_0(k))$, where δ_0 is the phase shift in the asymptotic $l = 0$ radial wavefunction.

2.3 Feshbach Interaction

Within the condensates we consider in this study, the interaction between particles can be controlled due to a phenomenon known as Feshbach resonance, which is the result of coupling between hyperfine levels, which are magnetically tunable via the Zeeman effect [11]. From 2nd order perturbation theory, it may be shown that by changing the magnetic B-field, a molecular state can be brought near resonance with the energy of the colliding atoms ($E \approx 0$), resulting in a scattering process whose scattering length near a resonance at B_0 is given by the formula

$$a(B) = a_{bg}\left(1 - \frac{\Delta B}{B - B_0}\right), \tag{2.28}$$

in which B_0 is the center of the resonance, ΔB the width of the resonance, and a_{bg} is the background scattering legnth, i.e. the scattering length between particles in the absence of a resonance [7, 11]. Note that the scattering length, which measures the strength of interaction between particles, diverges exactly at $B = B_0$. Therefore we introduce the notion of "unitarity", the regime in which $|na^3| \geq 1$, in which a Feshbach resonance causes significant interactions.

Because the significance of the scattering length is measured in relation to density, it is convenient at this point to introduce a density-dependent system of units, given by

$$\begin{aligned} E_n &= (6\pi^2 n)^{2/3}\frac{\hbar^2}{2\mu} \\ k_n &= \frac{\sqrt{2\mu E_n}}{\hbar} \\ t_n &= \frac{\hbar}{E_n}, \end{aligned}$$

where the single-particle number density n is assumed to be the same for both atoms (even if they are different species of atoms). This allows, for instance, to rewrite the unitarity condition as $|k_n a| \geq (6\pi^2)^{1/3} \approx 3.90$

Furthermore, the scattering length determines the existence of a two-particle bound state. When the scattering length is large and negative, and there is no weakly bound

state. However, with magnetic field below resonance, with large positive scattering length, there exists a weakly bound state, whose binding energy goes as $E_B = \frac{\hbar^2}{2\mu a}$ [10]. Rewriting this as well in terms of the density-dependent units, one finds the delightfully simple result $\frac{E_B}{E_n} = \frac{1}{(k_n a)^2}$. In this sense, the Feshbach energy spectrum as a function of scattering length for every Feshbach resonance is the same. We plot this spectrum in Fig. 2.5, where we parameterize the system in terms of $\frac{1}{a}$, because $\frac{1}{a}$ varies continuously as a function of B, as opposed to a itself, which diverges, and because it is precisely the divergence of a which we are interested in, thus mapping it to the origin makes it possible to plot. In Fig. 2.5, one clearly sees the bound state whose energy depends quadratically on $\frac{1}{a}$ for $\frac{1}{a} \to 0^+$.

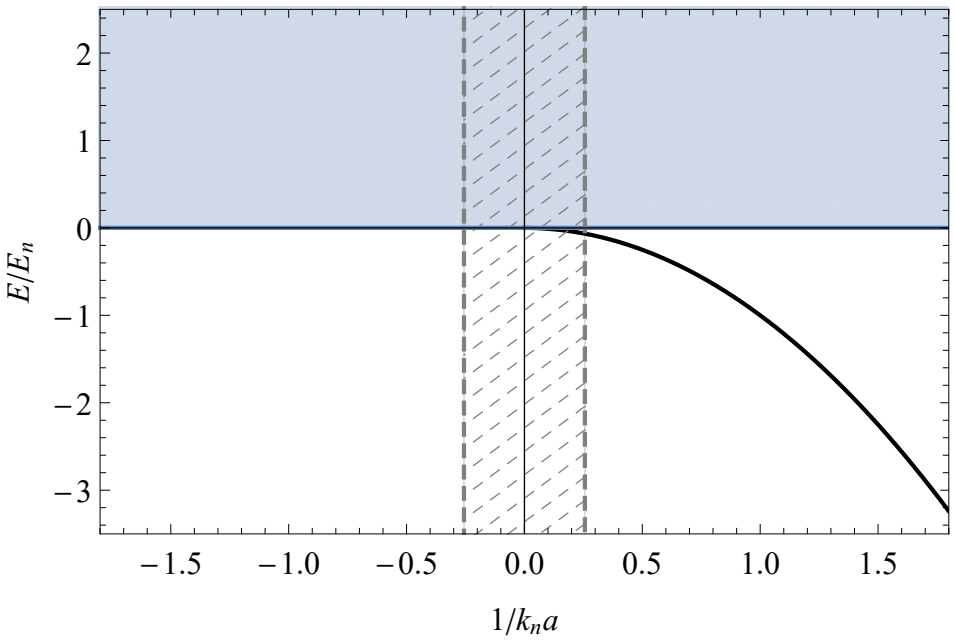

Figure 2.5: Energy spectrum of atoms interacting in free space due to a Feshbach resonance. The blue shaded region represents continuum (atomic) states, and the curve represents the bound (molecular) state with $\frac{E_B}{E_n} = \frac{1}{(k_n a)^2}$. Also, the dashed region in the center signifies the region of unitarity.

To model Feshbach interactions, we benefit from the concept of universality and are are free to use any potential which gives the correct scattering length and binding properties [11, 10]. A common, accurate model potential is the Lennard-Jones potential [10, 11, 7], whose

shape is adjusted to reproduce the appropriate scattering length.

Chapter 3

Calculations and Results

Having established the theoretical concepts used in our study, we now apply them to the scenario we wish to analyze: formation of interspecies Feshbach molecules in an ultracold Rb-K gas for the NASA CAL facility. We shall first describe the model we use to represent the behavior of the ultracold atoms, and then describe the results and analysis we obtained after computing the model for various parameters.

3.1 Model

In this study, we estimate the association of ^{87}Rb and ^{41}K atoms into Feshbach molecules in a dual-species ultracold gas. Following previous studies [4, 10], we adopt an effective model approach, focusing on the scattering behavior of a single Rb and single K atom. We will assume throughout that the number densities of Rb an K are equal. Then, after the B-field manipulation, the population of the 2-body wavefunction in a bound-state is taken to be equal to the molecular fraction of the entire gas.

3.1.1 Hamiltonian

We model the relative motion in the two-body scattering process by a Hamiltonian with an effective potential chosen to emulate two effects. Firstly, we impose a finite density constraint onto the system, by including a potential term for an artificial, spherically symmetric harmonic oscillator (in the relative frame), whose frequency is recast in terms of

trap length a_{ho}, an approach which has been demonstrated to be effective and accurate in Refs. [4, 12, 13, 14, 15, 16]. Specifically, we have

$$V_{ho}(r) = \frac{\hbar^2}{8\mu a_{ho}^4} r^2, \tag{3.1}$$

in which a_{ho} may be shown to be related to the (single-species) number density as

$$a_{ho} = \sqrt{\frac{\pi}{8}} \left(\frac{4\pi n}{3} \right)^{-1/3}. \tag{3.2}$$

With respect to the interatomic interactions, we use the standard Lennard-Jones potential (see Fig. 3.1),

$$V_{LJ}(r) = -\frac{C_6}{r^6} \left(1 - \frac{\lambda^6}{r^6} \right), \tag{3.3}$$

in which $C_6 = 4274$ in atomic units for ^{41}K-^{87}Rb [17], and λ is a tunable parameter adjusted to produce the desired value of the s-wave scattering length. Therefore, for a given B-field value to be modeled, we determine numerically the corresponding value of λ to produce the appropriate scattering length, according to Eq. (2.28).

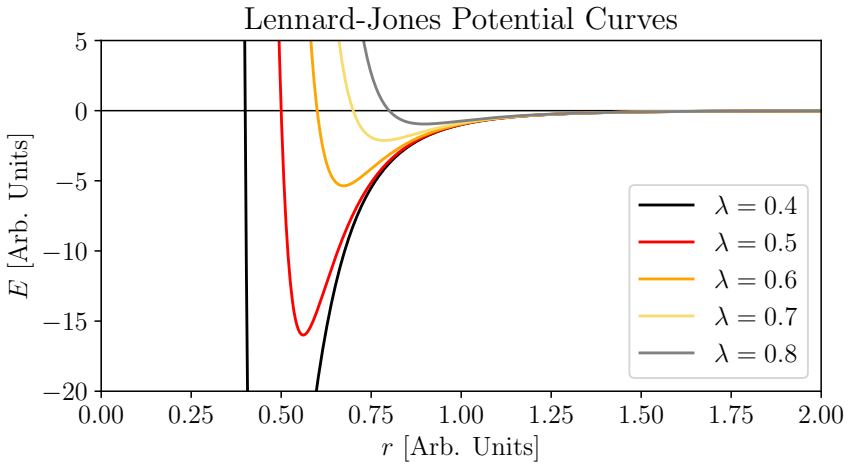

Figure 3.1: The Lennard-Jones potential for various values of λ. Note that λ determines the intercept on the r-axis.

Combining these potentials, we may write the ^{41}K-^{87}Rb relative Hamiltonian as

$$\hat{H} = -\frac{\hbar^2}{2\mu}\nabla^2 + \frac{\hbar^2}{8\mu a_{ho}^4} r^2 - \frac{C_6}{r^6} \left(1 - \frac{\lambda^6}{r^6} \right). \tag{3.4}$$

The spectrum of this Hamiltonian is shown in Fig. 3.2, in which one sees the discretization of the continuum arising from the harmonic oscillator potential, as well as the characteristic molecular state, like in Fig. 2.5.

Conversion of molecules from a (discretized) continuum state to a molecular state is only possible through a time-dependent process, since population in an eigenstate of the Hamiltonian cannot transfer to an eigenstate with different energy via a time-independent Hamiltonian. Therefore, in order to change atoms into molecules one must change the B-field in time from a configuration with $a < 0$ to a configuration with $a > 0$ admitting a weakly bound molecular state, a process in which energy is not conserved, and transfer from a continuum state to the ground state approaching 100% may occur. In order to determine the population of Feshbach molecules formed by a time-dependent process, we therefore solve numerically the time-dependent s-wave radial equation [18]

$$\left[-\frac{\hbar^2}{2\mu}\frac{1}{r}\frac{\partial^2}{\partial r^2}r + \frac{\hbar^2}{8\mu a_{ho}^4}r^2 - \frac{C_6}{r^6}\left(1 - \frac{\lambda(t)^6}{r^6}\right)\right]\psi(r,t) = i\hbar\frac{\partial}{\partial t}\psi(r,t) \tag{3.5}$$

beginning with the atoms entirely in the lowest energy state (since BECs are taken to be entirely in the ground state). This study will compare different schemes for the value of the B-field as a function of time.

To determine numerical solutions to Eq. (3.5), we first defined a discrete grid of scattering length values, at which to solve the corresponding time-independent Schrödinger equation (TISE). By expressing the basis functions $\phi_\beta(r)$ in a basis of B-splines, and truncating the basis states to a finite number of states (20 was found to be sufficient for the calculations in this study), one converts continuous operations to discrete matrix operations, thus allowing for one to solve the TISE as a matrix system. Thus, one may compute the eigenenergies (as seen in Fig. 3.2) and corresponding basis functions in the B-spline basis for each point in the scattering length grid.

Then, to solve the Time-Dependent Schrödinger Equations (TDSE) for this study, we follow methods based on the "Slow Variable Discretization" (SVD) method proposed in

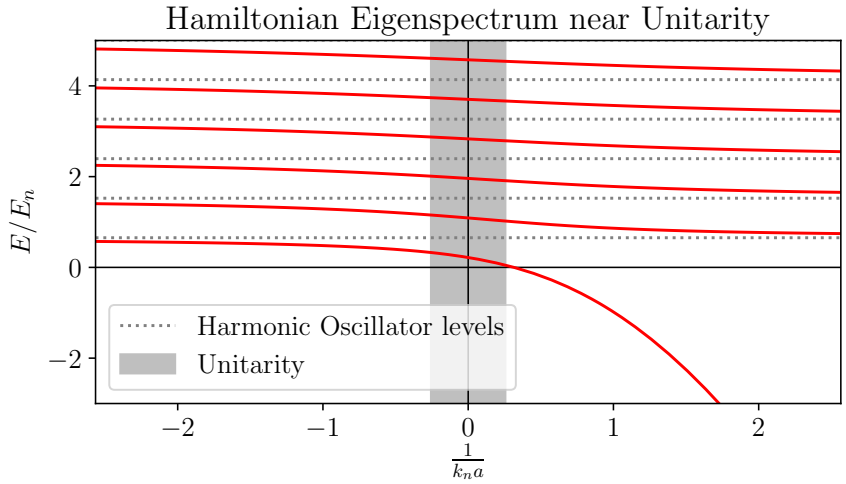

Figure 3.2: The energy levels of the Hamiltonian are shown parameterized by the inverse two-body scattering length a of the Lennard-Jones potential alone (determined by λ). In the limit of small $|a|$ (large $|\frac{1}{a}|$), the spectrum consists of pure harmonic oscillator levels, whose energies are plotted as dashed lines. Due to two-body universality, all densities have identical spectra when scaled by the density-dependent units. Positive energies correspond to atomic states, and negative energies represent molecular states. Note the similarities between this spectrum and that in Fig. 2.5

Ref. [19, 20]. To promote numerical stability, this method introduces another basis, the "Discrete Variable Representation" (DVR) basis, in which to express the time propagator. Thus, the time evolution is also converted to a matrix system which may be solved numerically.

To find the molecular fraction after changing B, at $t = t_f$, we expand the final state into the basis of eigenfunctions $\phi_\beta(r)$ of the Hamiltonian at times $t \geq t_f$, as $\psi(r,t) = \sum_{\beta\in\mathbb{N}} c_\beta \phi_\beta(r) e^{-iE_\beta(t-t_f)/\hbar}$, by computing the projections $c_\beta = \langle\phi_\beta(r)|\psi(r,t_f)\rangle$. Then, if the final B-field has $a > 0$ (as is typically chosen), $\beta = 0$ corresponds to the Feshbach molecule state having $E_B = -\frac{\hbar^2}{2\mu a^2}$, and we find that the molecular fraction of the K-Rb condensate is given simply by $|c_0|^2$.

3.1.2 B-field Sweeps and Quenches

Ultimately, the purpose of this study is to compare two molecule-creation schemes and investigate the trends of each. In order to create a basis for comparison, we choose

based on reasonable experimental parameters to study the properties of the first ^{41}K-^{87}Rb Feshbach resonance with both atoms in the $|F = 1, m_F = 1\rangle$ Zeeman level, occurring at $B = 39.4$ G [21], shown in Fig. 3.3. In each case, we select the initial and final scattering lengths to be $a_i = -2r_{vdW}$ and $a_f = 100r_{vdW}$, respectively, where the van der Waals length r_{vdW} is defined by $r_{vdW} = \frac{1}{2}\left(\frac{2\mu C_6}{\hbar^2}\right)^{1/4}$ [10]. This corresponds to B-field values of $B_i = 63.92$ G and $B_f = 37.89$ G. We note that the qualitative trends in our results do not depend on the particular choices of B_i and B_f, so long as they are chosen off resonance, i.e. $|a| \sim r_{vdW}$.

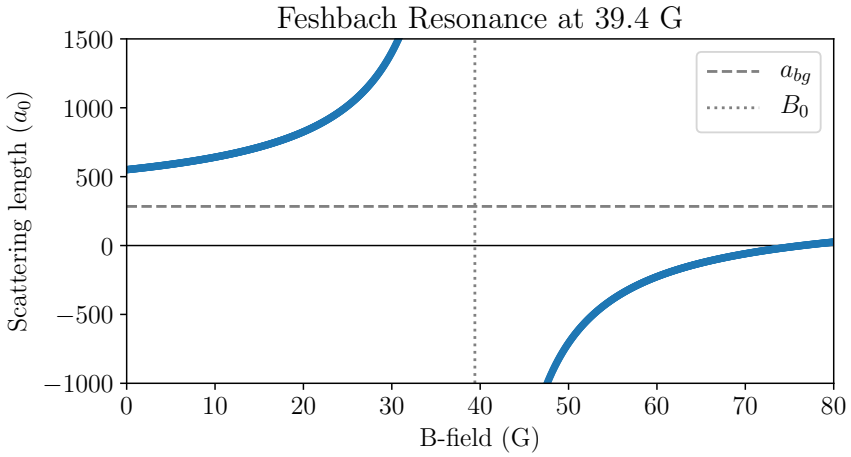

Figure 3.3: Scattering length as a function of applied B-field for the ^{41}K-^{87}Rb Feshbach resonance that occurs at 39.4 G. This resonance has $\Delta B = 37$ G and $a_{bg} = 284\ a_0$, where a_0 is the Bohr radius [21].

First, we explore a scheme consisting of a direct, linear sweep, characterized by sweeping the applied B-field linearly in time from B_i to B_f, passing over the resonance at B_0, where we parameterize the sweep by t_{sw}, the time spent sweeping. This is the scheme most commonly used at present in experiments.

The second scheme which we investigate consists of an instantaneous quench from B_i to B_0, followed by a period of dwell time t_{dw} spent with $B = B_0$, after which a linear sweep *from* B_0 *to* B_f is applied in time t_{sw}. Note that, although both schemes will be characterized by t_{sw}, it does not have identical meaning. This second scheme has been used experimentally before, though as far as we are aware, only with $t_{sw} = 0$ [22].

The two schemes are summarized graphically in Fig. 3.4. For this study, we wish to analyze which scheme can be more efficient at producing interspecies Feshbach molecules, particularly in short times, and at low densities.

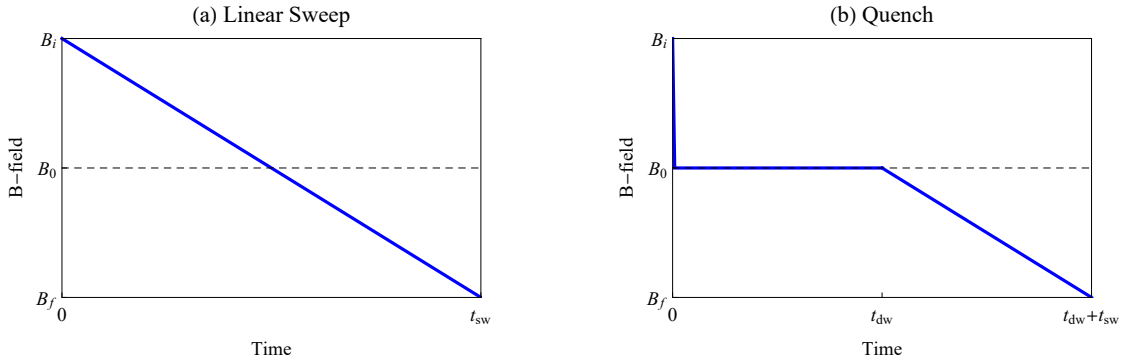

Figure 3.4: Schematic of magnetic field vs time in the linear sweep and quench schemes. In (a), the linear sweep changes the B-field directly from B_i to B_f linearly in time. In (b), the quench involves and instantaneous quench from B_i to B_0, followed by a linear sweep from B_0 to B_f. This schematic is not to scale, and B_i and B_f will not, in general, be equidistant from B_0, nor will t_{sw} and t_{dw} bear any particular relationship to each other.

As a result of the quantum adiabatic theorem, we should expect that, as $t_{sw} \to \infty$, the direct linear sweep will result in a molecular fraction approaching unity. Also, for the limit $t_{sw} \to 0$, we find the molecular fraction will be given by the projection of the initial state onto the Feshbach molecule eigenstate, usually approximately 0. Therefore, what we will be interested in understanding is whether in relatively short, finite time, the quenching scheme is capable of producing more molecules than a direct linear sweep.

3.2 Results

In order to investigate the trends of molecular creation in the linear scheme and quench scheme, we chose to compute the molecular formation rates for four different single-particle densities $n = n_{Rb} = n_K$: $n = 10^8$ cm^{-3}, $n = 10^9$ cm^{-3}, $n = 10^{10}$ cm^{-3}, and $n = 10^{11}$ cm^{-3}. For the CAL, lower densities are preferable, so we are most concerned with production of

molecules in the case that $n = 10^8$ cm^{-3}. In the following sections, we present both the results of our computations and a brief analysis of why they arise.

3.2.1 Absolute time analysis

We present the results of our computations solving the time-dependent Schrödinger equations in Fig. 3.5. These calculations yield two crucial observations, valid for all densities considered. First, when $t_{sw} = 0$ the fraction of molecules produced increases with t_{dw}, agreeing with the observations in Ref. [22].

Second, a nonzero t_{sw} in the quenching scheme improves the molecular fraction rate much more than the corresponding t_{sw} for a linear ramp. This immediately implies the most significant result of this thesis: within a given amount of time, a quench with finite t_{dw} followed by a non-instantaneous sweep away from unitarity will always produce a larger molecular fraction than the optimal (slowest) linear ramp in the same amount of time. Therefore, in order to produce as large a fraction of molecules as possible at low densities, we recommend that such a quench scheme be used, optimized to the loss timescales within a given experiment.

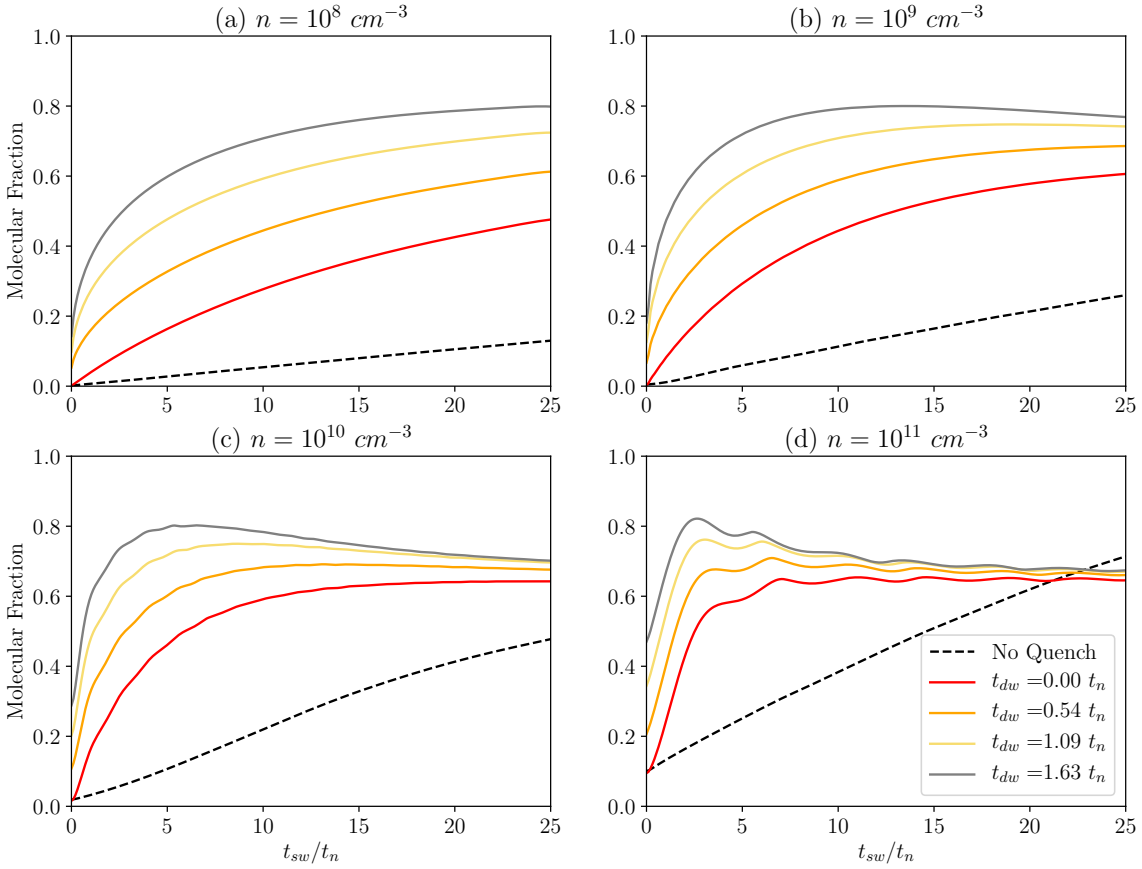

Figure 3.5: Fraction of molecules produced as a function of t_{sw} for various densities. The dashed curve is a direct sweep from $B_i = 63.92$ G to $B_f = 37.89$ G, and the dashed curves are quenches from B_i to $B_0 = 39.4$ G, followed by a sweep to B_f. Note that at $t_{sw} = 0$, the direct sweep is identical to a quench with $t_{dw} = 0$, so the corresponding curves intersect.

3.2.2 Unitarity analysis

To provide a qualitative argument why the results in Sec. 3.2.1 occur, we propose that one of the important factors that drives a 2-body system to produce Feshbach molecules is the time spent sweeping at unitarity, where the interactions between particles are most important. Therefore, we define t_u to be the amount of time spent sweeping at unitarity (but *not* including dwelling), and reformulate the results from Sec. 3.2.1 in terms of the ratio t_u/t_n, plotted in Fig. 3.6. On this timescale, one sees that, except for $n = 10^{11}$ cm^{-3},

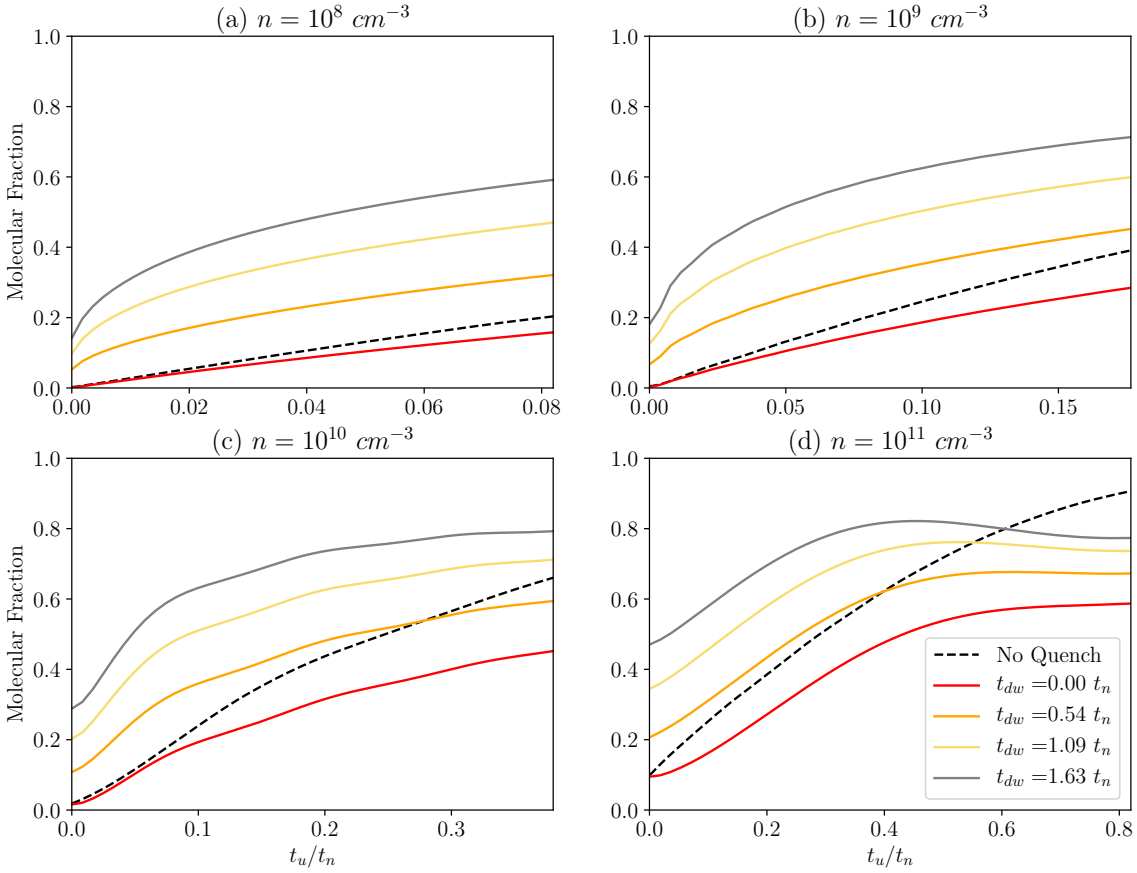

Figure 3.6: Fraction of molecules produced as a function of t_u, the amount of time with $|na^3| \geq 1$. These are the same results as shown in Fig. 3.5, but with the sweeps and quenches rescaled by the proportion of time spent at unitarity during the sweep. One finds some noticeably different behavior for the linear sweep in (d) compared to the other curves. This is due to the large density, which is not the focus of this study.

there is a strong correspondence between the quench with $t_{dw} = 0$ and the linear sweep at the same t_u/t_n for small times. Furthermore the quench curves with nonzero t_{dw} provide primarily a constant offset, and exhibit closely matching trends in molecular fraction as a function of t_u/t_n relative to each other.

Chapter 4

Conclusion

This thesis has investigated methods to produce molecules via Feshbach resonance, focusing on the regime relevant to production of molecules at low density in a microgravity environment. Based on the trends discovered from our computations, we conclude that a quench scheme can generally be made superior to a linear sweep. In addition to agreeing qualitatively with the results in Ref. [22], we predict that further optimization is possible by introducing a linear sweep after the quench. With respect to the NASA CAL experiment, this will be essential, since insufficient molecules ($< 20\%$) are created in reasonable amounts of time using the linear sweep at the desired low density of $n = 10^8$ cm^{-3}.

In further studies of molecular production, several more complicated aspects of the system could be investigated. For instance, one could introduce various loss rate models dependent on scattering length, and attempt to optimize molecular production constrained by the loss timescales. Also, while the analysis in this thesis considered purely 2-body interactions, one could extend the analysis by computing 3-body effects, which would then have to consider both Rb-Rb-K and Rb-K-K interactions, as well as introduce a loss mechanism.

References

[1] NASA, "Cold Atom Laboratory: The Coolest Spot in the Universe," 2019.

[2] D. Schlippert, J. Hartwig, H. Albers, L. L. Richardson, C. Schubert, A. Roura, W. P. Schleich, W. Ertmer, and E. M. Rasel, "Quantum Test of the Universality of Free Fall," Phys. Rev. Lett., vol. 112, p. 203002, May 2014.

[3] P. Touboul, G. Métris, V. Lebat, and A. Robert, "The MICROSCOPE experiment, ready for the in-orbit test of the equivalence principle," Classical and Quantum Gravity, vol. 29, p. 184010, aug 2012.

[4] J. P. D'Incao, M. Krutzik, E. Elliott, and J. R. Williams, "Enhanced association and dissociation of heteronuclear Feshbach molecules in a microgravity environment," Phys. Rev. A, vol. 95, p. 012701, Jan 2017.

[5] Williams, J. R., and D'Incao, J. P., unpublished.

[6] D. Schroeder, An Introduction to Thermal Physics. Addison Wesley, 1999.

[7] C. J. Pethick and H. Smith, Bose-Einstein Condensation in Dilute Gases. Cambridge University Press, 2 ed., 2008.

[8] L. Landau and E. Lifshitz, Quantum Mechanics: Non-Relativistic Theory. Course of Theoretical Physics, Elsevier Science, 1981.

[9] D. McIntyre, C. Manogue, J. Tate, and O. S. University, Quantum Mechanics: A Paradigms Approach. Always learning, Pearson, 2012.

[10] J. P. D'Incao, "Few-body physics in resonantly interacting ultracold quantum gases," Journal of Physics B: Atomic, Molecular and Optical Physics, vol. 51, p. 043001, jan 2018.

[11] C. Chin, R. Grimm, P. Julienne, and E. Tiesinga, "Feshbach resonances in ultracold gases," Rev. Mod. Phys., vol. 82, pp. 1225–1286, Apr 2010.

[12] B. Borca, D. Blume, and C. H. Greene, "A two-atom picture of coherent atom–molecule quantum beats," New Journal of Physics, vol. 5, pp. 111–111, sep 2003.

[13] K. Góral, T. Khler, S. A. Gardiner, E. Tiesinga, and P. S. Julienne, "Adiabatic association of ultracold molecules via magnetic-field tunable interactions," Journal of Physics B: Atomic, Molecular and Optical Physics, vol. 37, pp. 3457–3500, aug 2004.

[14] J. von Stecher and C. H. Greene, "Spectrum and Dynamics of the BCS-BEC Crossover from a Few-Body Perspective," Phys. Rev. Lett., vol. 99, p. 090402, Aug 2007.

[15] A. G. Sykes, J. P. Corson, J. P. D'Incao, A. P. Koller, C. H. Greene, A. M. Rey, K. R. A. Hazzard, and J. L. Bohn, "Quenching to unitarity: Quantum dynamics in a three-dimensional Bose gas," Phys. Rev. A, vol. 89, p. 021601, Feb 2014.

[16] J. P. Corson and J. L. Bohn, "Bound-state signatures in quenched Bose-Einstein condensates," Phys. Rev. A, vol. 91, p. 013616, Jan 2015.

[17] A. Derevianko, J. F. Babb, and A. Dalgarno, "High-precision calculations of van der Waals coefficients for heteronuclear alkali-metal dimers," Phys. Rev. A, vol. 63, p. 052704, Apr 2001.

[18] J. P. D'Incao, J. Wang, and V. E. Colussi, "Efimov Physics in Quenched Unitary Bose Gases," Phys. Rev. Lett., vol. 121, p. 023401, Jul 2018.

[19] O. I. Tolstikhin, S. Watanabe, and M. Matsuzawa, "'Slow' variable discretization: a novel approach for Hamiltonians allowing adiabatic separation of variables," Journal of Physics B: Atomic, Molecular and Optical Physics, vol. 29, pp. L389–L395, jun 1996.

[20] J. E. Bækhøj, O. I. Tolstikhin, and L. B. Madsen, "'Slow' time discretization: a versatile time propagator for the time-dependent Schrdinger equation," vol. 47, p. 075007, mar 2014.

[21] A. Simoni, M. Zaccanti, C. D'Errico, M. Fattori, G. Roati, M. Inguscio, and G. Modugno, "Near-threshold model for ultracold KRb dimers from interisotope Feshbach spectroscopy," Phys. Rev. A, vol. 77, p. 052705, May 2008.

[22] M. Mark, T. Kraemer, J. Herbig, C. Chin, H.-C. Ngerl, and R. Grimm, "Efficient creation of molecules from a cesium Bose-Einstein condensate," Europhysics Letters (EPL), vol. 69, pp. 706–712, mar 2005.